# Structure of poly(ionic liquid)s in solutions: a small angle scattering study

Carlos G. Lopez,[1] Atsushi Matsumoto,[2] Anish Gulati,[1] Can Hou,[1] Yuna Mizutani,[3] Hiroto Osada,[2] Yume Tao,[3] Kakeru Fujii,[3] Walter Richtering,[1,4] and Takaichi Watanabe[3]

[1)] *Institute of Physical Chemistry, RWTH Aachen University, 52056 Aachen, Germany, European Union*[a)]

[2)] *Department of Applied Chemistry and Biotechnology, University of Fukui, Fukui 910-8507, Japan*[b)]

[3)] *Department of Applied Chemistry, Graduate School of Natural Science, Okayama University, 3-1-1, Tsushima-naka, Kita-ku, Okayama 700-8530, Japan*

[4)] *DWI—Leibniz-Institute for Interactive Materials e.V., RWTH-Aachen University, Forckenbeckstraße 50, 52074 Aachen, Germany, European Union*

We investigate the phase behaviour and scattering properties of a polymerised ionic liquid (poly(1-butyl-3-vinylimidazolium bis(trifluoromethanesulfonyl)imide)) in 24 solvents of varying dielectric constants and solubility parameters. The polymer is found to be soluble in polar aprotic solvents and insoluble in non-polar or highly protic solvents. Three types of behaviour can be observed: in high permittivity solvents, the correlation length is inversely proportional to the square root of the concentration $c$, and the proportionality constant decreases with solvent permittivity if the Bjerrum length is larger than $\simeq 1$ nm. For solvents with modest dielectric permittivities ($\epsilon \simeq 18 - 30$), the correlation length scales as $\xi \propto c^{-1/3}$, suggesting a pearl-necklace conformation. Finally, in THF, the scattering pattern follows the Ornstein-Zernike behaviour. The scaling of the correlation length and zero-angle scattering intensity are similar to those of neutral polymers in good solvents. The results are compared with scaling models for solvophilic and solvophobic polyelectrolytes.

## I. INTRODUCTION

Ionic liquids are molten salts consisting of organic cations and organic or inorganic fluorinated anions.[1] When ionic liquid ions are covalently bound to polymer repeating units, the resultant polymer is called poly(ionic liquid) or polymerized ionic liquid.[2] Poly(ionic liquid)s (PILs) combine the unique physico-chemical properties of ionic liquids (e.g., high ionic conductivity, $CO_2$ absorption, antimicrobial) with the attractive mechanical properties of polymers.[3] This has made PILs appealing materials for various applications, such as electrolytes in batteries,[4] lubricant additives for coating,[5] membranes for molecular separation[6] catalysts for chemical reactions[7] as well as stabilizers for particles in solutions.[8] Consequently, understanding the conformation of PILs in solution or bulk state is an inevitable step to control the material properties of PILs-based materials.

Since PILs possess dissociable counterions, the conformation of PILs in solution may be explained within the framework of molecular models proposed for polyelectrolytes in solution.[9,10] Several research groups investigated the viscosity for PIL solutions.[11–14] For example, Chen and Elabd[11] showed that the specific viscosity ($\eta_{sp}$) of their PIL was proportional to the square root of the polymer concentration in the semidilute unentangled regime. The observed power-law dependence is known as the Fuoss law[15] and agrees with the predicted scaling law for salt-free polyelectrolyte solutions.[16,17] These results indicate that the conformation of PILs is strongly influenced by strong electrostatic interactions, similar to that for conventional polyelectrolytes (CPEs), such as poly(sodium styrenesulfonate)[18–20] and sodium carboxymethyl cellulose.[21–23]

To further study the effect of the electrostatic interactions on the solution viscosity of PILs, Matsumoto et al.[24] have recently investigated the effect of the solvent dielectric constant on the specific viscosity of a PIL, poly(1-butyl-3-vinylimidazolium bis(trifluoromethanesulfonyl)imide) ($PC_4$-TFSI), in the semidilute unentangled regime. The dielectric constant ($\varepsilon$) is a key parameter in polyelectrolyte solutions because it modifies the strength of electrostatic interactions. This is usually quantified through the Bjerrum length, which is the distance at which electrostatic forces between two monovalent ions are equal to the thermal force:

$$l_B = \frac{e^2}{4\pi\varepsilon\varepsilon_0 k_B T}, \tag{1}$$

where $e$ is the electrostatic unit of charge, $k_B$ the Boltzmann constant, $T$ the absolute temperature, $\varepsilon$ the relative dielectric constant of solvents, and $\varepsilon_0$ the vacuum permittivity. According to the Oosawa-Manning theory, the magnitude of $l_B$ relates to the number of dissociated counterions, i.e., the charge fraction, through

$$f = \frac{b}{l_B}, \tag{2}$$

where $b$ is the distance between charges. Therefore, the higher the solvent dielectric constant, the larger the charge fraction is predicted. When the charge fraction increases, the end-to-end distance of polyelectrolyte chains increases due to strong electrostatic repulsion between

[a)] Current address: Materials Science and Engineering Department, The Pennsylvania State University, University Park, Pennsylvania 16802, United States; These two authors contributed equally

[b)] These two authors contributed equally

charged groups on the chain backbone. Thus, it is anticipated that the specific viscosity is larger for solvents with higher solvent dielectric constants. Indeed, Matsumoto et al. found that the specific viscosity increased with increasing the solvent dielectric constant, the trend apparently agreeing with Eq. 2. However, we should note that the change in solvent species alters also the strength of the excluded volume interaction. For example, Jousset et al. showed that the specific viscosity of their PIL in $N$-methylformamide ($\varepsilon = 180$) was smaller than that in $N, N$-dimethylformamide ($\varepsilon = 38$), indicating clearly the presence of the solvent quality effect.

Scattering experiments to measure the correlation length of polyelectrolytes in semidilute regime could be a powerful method to test separately the influence of solvent quality and dielectric constant on the conformation of polyelectrolytes. In good solvents, the solvent quality contribution is less important, and thus polyelectrolyte chains are extended by the electrostatic interactions.[10] The correlation length in good solvents is predicted to be scaled as $\xi \propto c^{-1/2}$ against the polymer concentration. On the other hand, in poor solvents, the solvent quality contribution is no longer negligible because the polymer/solvent interfacial energy is comparable to the electrostatic energy. According to the Dobrynin and Rubinstein model,[9] polyelectrolytes in poor solvents are depicted as a nacklace-like chain consisting of compact beads connected with narrow strings. They found that the semidilute regime was divided into two different regimes: string-controlled regime and bead-controlled regime. In the string-controlled regime, the model predicts the same $c^{-1/2}$ dependence for $\xi$ as in good solvents. The difference is that the increase in $\xi$ in poor solvents is caused by the decrease in the exclude volume. In the beads-controlled regime, the solvent quality contribution becomes dominant, and the correlation length is predicted to show a weaker dependence of $\xi \propto c^{-1/3}$. Accordingly, the solvent quality can be quantified by measuring the correlation length of PILs at different polymer concentrations.

Motivated by the discussion above, we investigate the phase behavior and scattering properties of $PC_4$-TFSI in a broad set of organic solvents of varying dielectric constant. We establish the scaling of the correlation length with Bjerrum length and compare our results with various scaling models. In high dielectric constant solvents, $PC_4$-TFSI behaves displays typical polyelectrolyte behaviour: the correlation length scales with concentration as $\xi \propto c^{-1/2}$, as has been observed for many systems before. For intermediate dielectric constant solvents, we find $\xi \propto c^{-1/3}$, which we rationalise as arising from polyelectrolyte collapse. Finally, in THF, neutral polymer behaviour is observed, in agreement with viscosity results from an earlier publication.[24] The results help establish a framework for the effects of electrostatics and solvent quality on the solution properties of polyelectrolytes.

## II. MATERIALS AND METHODS

**Chemicals:** The solvents purchased from different manufacturers were used without further purification. Conductivity measurements were used to estimate the levels of ionic impurities.

*Polymer synthesis:* 1-Vinylimidazole and Lithium bis(trifluoromethanesulfonyl)imide (Li-TFSI) were purchased from Tokyo Chemical Industry, Japan. 1-Bromobutane, methanol, 2,2'-azobis(isobutyronitrile) (AIBN), and silver nitrate ($AgNO_3$) were purchased from FUJIFILM Wako Chemicals, Japan. 1- Vinylimidazole was used after distillation at 85°C under vacuum to remove inhibitors contained in the as-received product. Deionized (DI) water was obtained from a water purification system (ICW-3000, Merck).

*Solvents for small angle x-ray scattering (SAXS):* 3-Methylsulfolane (3-MS), methyl ethyl ketone (MEK), *tert*-butyl acetoacetate (t-BAA), triethyl phosphate (TEP) were purchased from Tokyo Chemical Industry, Japan. Dimethylformamide (DMF), methanol (MeOH), $N$-methylformamide (NMF), propylene carbonate (PC), dimethyl sulfoxide (DMSO), tetrahydrofuran (THF), acetonitrile (ACN), nitromethane (NM), nitrobenzene (NB), acetone (AC), formamide (F), and pyridine (P) were purchased from FUJIFILM Wako Chemicals, Japan. Super dehydrated products were commercially available and thus used for DMF, MeOH, DMSO, THF, ACN, AC. 1-Nitropropane (1-NP), N-Methyl-2-pyrrolidone (NMP), benzaldehyde (BA), 2-pentanone (2-P), 3-pentanone (3-P), methyl isobutyl ketone (MIBK) and ethylene glycol monomethyl ether (EGME) and ethylene carbonate (EC) were purchased from VWR.

*Solvents for small angle neutron scattering (SANS):* The deuterated solvents used for the SANS measurements were purchased from Deutero GmbH. The solvent grades have been given in table II.

| Solvent | Purity [%] | Deuteration [%] |
|---|---|---|
| Acetone | 99.8 | 99.0 |
| Acetonitrile | 99.8 | 99.0 |
| DMF | 99.5 | 99.0 |
| DMSO | 99.8 | 99.0 |
| Methanol | 99.8 | 99.5 |
| Nitrobenzene | 99.5 | 99.0 |
| Nitromethane | 99 | 99.0 |
| THF | 99.5 | 99.0 |

TABLE I. Deuterated solvents used for small-angle neutron scattering experiments.

**Poly(ionic liquid) synthesis:** Polyl(1-butyl-3-vinylimidazolium bis(trifluoromethanesulfonyl)imide ($PC_4$-TFSI) was obtained following the synthetic route used in our previous work.[24] Specifically, the monomer of 1-butyl-3-vinylimidazolium bromide ($C_4$-Br) was

first synthesized by refluxing 1-vinylimidazole with an excess amount of 1-bromobutane in methanol at 60°C for 3 days. The molar ratio of 1-bromobutane to 1-vinylimidazole and the solvent weight fraction were set at 1.2 and 0.17, respectively. After removing unreacted 1-bromobutane and solvent methanol at 50°C under vacuum, a viscous yellowish solution of $C_4$-Br was obtained. The purity of $C_4$-Br was confirmed using $^1$H-NMR in deuterated acetone.

Subsequently, the obtained $C_4$-Br was polymerized via free radical polymerization in DI water at 60°C for 1 day using an initiator of AIBN. The molar ration of the initiator to the monomer was set at 0.02, and the molar concentration of $C_4$-Br was 1.8 mol/L. After polymerization, a yellowish gel was formed, and the unreacted monomers and short chain oligomers were removed through a tube dialysis procedure against water. The dialysis was continued using a dialysis tube (Spectra Por 3, Fisher Scientific Japan) until the ionic conductivity of the solvent became lower than 4 $\mu$S/cm, a conductivity level for DI water reaching when it is exposed to air in our laboratory. The nominal molecular cutoff of the dialysis tube specified by the manufacturer was 3500. The resultant polymer solution was dried using a freeze-drying method, and poly(1-butyl-3-vinylimidazolium bromide) ($PC_4$-Br) was obtained in a fluffy cotton-like form.

Finally, $PC_4$-TFSI was prepared through a counterion metathesis reaction proposed by Marcilla et al.[25] Namely, bromide ions were exchanged to TFSI ions by slowly titrating an aqueous solution of Li-TFSI into an aqueous solution of $PC_4$-Br. The molar ratio of TFSI anions to Br anions was set at 1.2, while the molar concentration of $PC_4$-Br monomers and Li-TFSI were 0.15 mol/L and 0.55 mol/L, respectively. After the counterion conversion reaction, the precipitate, i.e., $PC_4$-TFSI, was formed and washed with deionized water until the filtrate remained transparent when adding an aqueous solution containing 0.1 mol/L of $AgNO_3$ to confirm the sufficient removal of bromide ions from the precipitate.

**SAXS measurements:** Test solutions were prepared by directly mixing the components into a glass vial at a designed $PC_4$-TFSI concentration ranging from 3 g/L to 200 g/L. The obtained polymer solution was then loaded into quartz capillaries (WJM Glas Müller GmbH) with internal diameters of 1.5 or 2 mm. Solutions containing volatile solvents were sealed using an epoxy glue gun to prevent evaporation. Measurements were carried out with the following three instruments:

*In-house instruments:* Measurements on a *Nano – inXider* instrument from *Xenocs* were performed at the DWI – Leibniz-Institut für Interaktive Materialien e.V, Aachen, Germany. This instrument used a Cu source and Dectris Pilatus 3 hybrid photon counting detector. The SDD was 938 mm. A beam wavelength of 1.54 Å was used. The accessible scattering vector range is 0.011 $nm^{-1} < q < 4.4$ $nm^{-1}$. Radial averaging and empty capillary subtraction was carried out using the manufacturer's software Nano-inXider Version 2.3.2, whereby the data is saved as .edf files, which is compatible with the manufacturer's XSACT software for further analysis, as well as .dat files, which are analogous to .txt files.

*SPring-8:* Samples at BL40B2 were loaded one at a time onto a custom in-house sample holder. The detector distance was to set to 4m, corresponding to a $q$-range of 0.023 $nm^{-1}$ <; $q$ <; 2.0 $nm^{-1}$, while the beam energy was set to 10 KeV. Most of the samples was then exposed to the beam for 10 seconds, except for DMSO samples, which exposed for more than 5 minutes due to the low transmission. The temperature was controlled by a Peltier heating unit to 25 °C.

*Diamond light source:* Samples at the I22 beamline were loaded onto a custom-made multi-slot holder. Samples were measured at room temperature $\simeq$ 23 °C. The accessible $q$-range was 0.016 $nm^{-1} < q < 1.6$ $nm^{-1}$. The data were reduced with standard procedures and masking. In the case of I22, the reduction was done through the Data Analysis WorkbeNch (DAWN) software. The data from I22 were further treated by subtracting the empty cell reading, which was considered to be the background.

**SANS measurements:** All SANS samples were measured in quartz cells with path-lengths of 1 mm, 2 mm or 5 mm depending on the polymer concentration, with less concentrated samples being measured in thicker cells. Data reduction was carried out according to the standard procedures at the various neutron facilities.

*TAIKAN:* The TAIKAN instrument at the JPARC neutron facility was used with a sample-to-detector distance of 5.65 m and a wavelength rage of 1.75 Å, giving a $q$-range of $\simeq 0.005$ $Å^{-1} < q < 0.7$ $Å^{-1}$. Data were put onto an absolute scale by using glassy carbon as a standard.

*SANS2D and ZOOM:* Some of the SANS measurements were carried out at the SANS2D and ZOOM instruments at the ISIS neutron and muon source. The SANS2D is a time-of-flight instrument consisting of two $^3$He-$CF_4$-filled ORDELA detectors, each with an active area of 96.5 cm × 96.5 cm. The sample-to-detector distance (SDD) for the rear detector was set to 4 m, which covered a $q$-range of 0.0045 $Å^{-1}$ to 1 $Å^{-1}$. The ZOOM instrument has a movable detector comprising an array of 192, 1 m long, 8 mm in diameter $^3$He tubes. The SDD for this instrument was kept at 4 m covering a $q$-range of 0.0045 $Å^{-1}$ to 0.85 $Å^{-1}$.

**Densitometry:** The density measurements were made using the Anton Paar DMA 5000 densitometer. The instrument had a least count of $10^{-6}$ g $cm^{-3}$. The instrument accuracy was routinely checked using deionized water. The samples for these measurements were prepared in glass vials, sealed using parafilm and allowed to dissolve overnight. Results are presented in the supporting information.

**Phase mapping:** The polymer powder was mixed with a given solvent at a concentration of 1wt% in a glass vial

and allowed to mix on a roller mixer or a vortexer over a period of up to two weeks. The dissolution state of the polymer was evaluated visually, as explained in the results section.

## III. BACKGROUND THEORY

The scaling model of Dobrynin et al.[16,17] calculates the conformation of polyelectrolyte using the concept of the electrostatic blob, which is the distance at which the Coulomb energy of $g_{\mathrm{el}}$ monomers is equal to the thermal energy $\simeq k_{\mathrm{B}}T$. The conformation of the $g_{\mathrm{el}}$ monomers which make up the electrostatic blob of size $\xi_{\mathrm{el}}$ is assumed to be unaffected by electrostatics and depends only on the solvent quality. On distances larger than the electrostatic blob but smaller than the electrostatic screening length, chains are predicted to adopt either a rigid or directed random walk conformation.

For salt-free semidilute solutions, the scaling theory of Dobrynin et al.[16,17] expects that electrostatic screening occurs at a length-scale $\xi$, known as the correlation length or mesh size. Specifically, the model predicts the correlation length to scale as:

$$\xi = \left(\frac{B}{bc}\right)^{1/2} \tag{3}$$

where $b$ is the length of a chemical monomer, which for our system matches the distances between charges, $c$ is the concentration of chemical monomers in units of number per unit volume and $B$ is a parameter equivalent to the ratio of the contour length of a correlation blob to the end-to-end distance of the correlation blob. If the chain is fully stretched inside the correlation blob then $B = 1$. Values of $B$ larger than 1 indicate coiling inside the correlation blob.

For polyelectrolytes with fewer than one dissociated charge per Kuhn segment, the scaling model predicts:

$$B \propto \begin{cases} l_{\mathrm{B}}^{-2/3} A^{4/3} & \text{for } T \ll \theta, \quad (4a) \\ l_{\mathrm{B}}^{-1/3} A^{2/3} & \text{for } T = \theta, \quad (4b) \\ l_{\mathrm{B}}^{-2/7} A^{4/7} & \text{for } T > \theta \quad (4c) \end{cases}$$

where $A$ is the number of monomers between dissociated charges, $\theta$ the theta temperature, $\xi_{\mathrm{T}}$ the thermal blob size and $u = l_{\mathrm{B}}/b$.

According to the Manning condensation model,[26] for highly charged polyelectrolytes, there is one dissociated charge per Bjerrum length. All other charges are predicted to condense on the polymer backbone. Therefore, Manning's theory expects $A \simeq l_{\mathrm{B}}/b$. When there is more than one dissociated charge per Kuhn segment ($l_{\mathrm{B}} \lesssim l_{\mathrm{K}}$), the electrostatic blob size is of the order of the Bjerrum length ($\xi_{\mathrm{el}} \simeq l_{\mathrm{B}}$). In this case, the conformation inside the electrostatic blob is expected to be rigid due to the intrinsic (non-electrostatic) stiffness of the backbone. The stretching parameter parameter is then expected to be $B = 1$ if no transverse fluctuations are assumed to take place on lengthscales between $\xi_{\mathrm{el}}$ and $\xi$ (i.e. electrostatic blobs are aligned into a rod-like configuration inside the correlation blob).

## IV. RESULTS AND DATA ANALYSIS

### Phase behaviour

The solubility of the $PC_4$-TFSI at a concentration of $\simeq$ 1wt% was tested in 50 solvents. The results are listed in the supporting information. We divide the solubility behaviour into three classes: First, samples which form clear solutions are classified as 'soluble'. Samples where the polymer powder is not swollen or dissolved by the solvent are classified at 'insoluble'. Lastly, samples where we observe either the formation of swollen gel phase coexisting with a solvent rich phase or turbid solutions are classified as 'partially soluble'. Tab. S1 lists the results of the solubility tests along with the dielectric constant and the Hansen solubility parameters of each solvent. Values for these were obtained from refs. [ 27].

### Small angle scattering

The recorded scattering curves obtained can be divided into three types: 1) samples displaying a peak, 2) samples displaying a broad shoulder and 3) samples displaying an Ornstein-Zernike behaviour. We consider these in turn.

For samples displaying a clear maximum in their scattering function, the data were visually trimmed and a polynomial function was fitted around the peak position and the scattering vector at the maximum $q^*$ was determined. An example of this type of fit is shown in Fig. 1a for solution in DMF at various $PC_4$-TFSI concentrations. The best-fit parameters of the polynomial are provided in the supporting information. The correlation length of these solutions was then estimated as:

$$\xi = \frac{2\pi}{q^*} \tag{5}$$

For samples displaying a broad shoulder, the correlation length was extracted using the method of Salamon et al.[28] Here, two linear functions were fitted to the data, as shown in Fig. 1b for solutions in acetone at different concentrations. The intercept between these two lines was taken as $q^*$ and the value of $\xi$ was calculated using Eq. 5.

The scattering pattern of THF solutions and some pyridine solutions were described by the Ornstein-Zernike function:[29,30]

$$I(q) = \frac{I(0)}{1 + (q\xi_{\mathrm{OZ}})^2} + C \tag{6}$$

where $I(0)$ is the scattering intensity at zero angle, $\xi_{OZ}$ is the correlation length and $C$ is a term that accounts

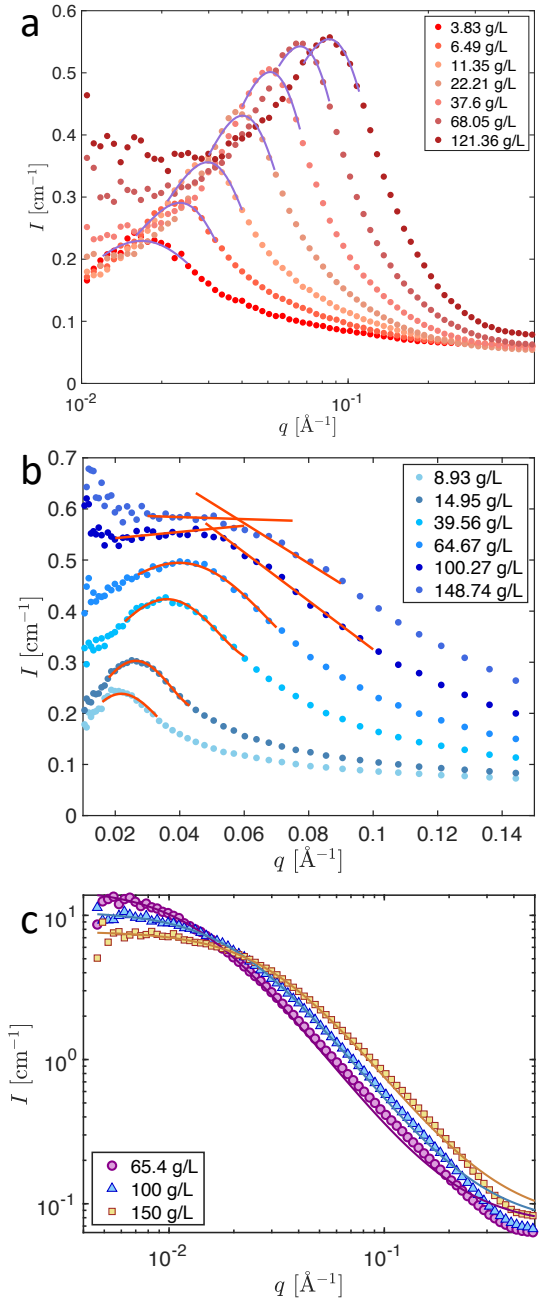


FIG. 1. Fits to small angle neutron scattering data. a: For d-DMF solutions a polynomial fit around the maxima, shown by the full lines, is used to extract the peak position. b: Solutions in d-acetone display a peak to shoulder transition. When peaks are not clearly distinguishable, as for the two highest concentrations plotted, two linear functions are used to extract the position of the shoulder. c: d-THF solutions are fitted to Eq. 6, shown by the full line.

for $q$-independent scattering, which for neutrons arises primarily due to spin incoherence. Eq. 6 is known to describe the scattering behaviour of neutral polymers in good solvents[29–31] and polyelectrolytes in excess added salt.[32,33] As shown in figure 1c, Eq. 6 provides a good description of the SANS intensity of $PC_4$-TFSI solutions in deuterated THF.

All the $I$ vs. $q$ scattering data are included as a supplementary spreadsheet.

## V. DISCUSSION

### A. Phase behaviour

$PC_4$-TFSI was found to be generally insoluble in polar protic solvents such as alcohols, diols or water, with the exception of methanol. Highly non-polar solvents such as benzene, toluene or cyclohexane also did not solubilise the polymer. Polar solvents of modest proticity, including several ketones, aldehydes and amides on the other hand tended to dissolve the polymer.

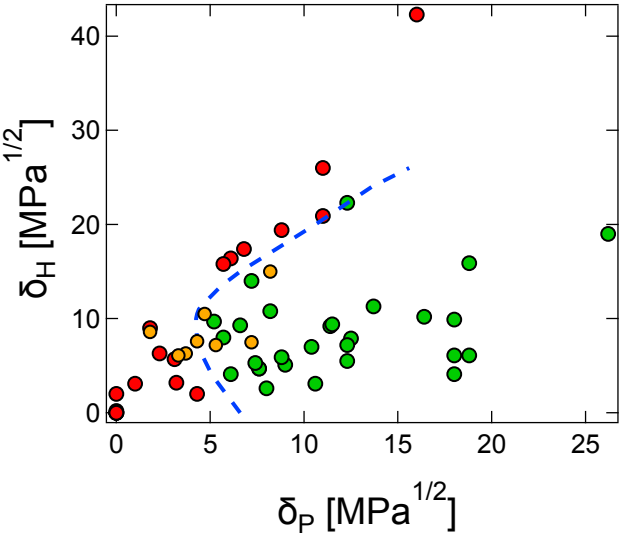


FIG. 2. Solubility behaviour of PIL in various solvents. For each solvent, the H-bonding Hansen solubility parameter ($\delta_H$) is plotted against the dipolar Hansen solubility parameter ($\delta_P$). Green circles indicate PIL is soluble in a given solvent and red circles indicate that is is insoluble. Yellow circles are for solvents which swell or partially dissolve the polymer, see the text for details. Blue line is estimate of boundary separating the soluble and insoluble regions.

We apply the Hansen solubility framework to the $PC_4$-TFSI in Fig. 2, which plots the hydrogen bonding component of the Hansen solubility parameter ($\delta_H$) vs. the dipolar component ($\delta_P$). The contribution of the dispersion term is not considered here. A soluble region (green symbols) is observed for high $\delta_P$, low $\delta_H$ region, consistent with the qualitative observations outlined above. The blue dashed line represents an approximate boundary dividing the soluble and insoluble regions. We note that the boundary appears to be somewhat diffuse, with partially soluble systems being observed in either side of

it.

Simple scaling models, which do not consider the influence of ion-solvent and polymer solvent interactions in detail expect the dielectric constant to be the main driving factor for polyelectrolyte dissolution, as this parameter controls the fraction of counterions which can dissociate from the backbone. For the system studied here, it seems clear that the dielectric constant alone is not a useful predictor of solubility: several high dielectric constant solvents such as water ($\epsilon \simeq 80$) and ethylene glycol ($\epsilon \simeq 37$) do not dissolve the polymer but others with modest permittivities such as THF ($\epsilon \simeq 8$), pyridine ($\epsilon \simeq 12$) or 2-pentanone ($\epsilon \simeq 16$) do.

Considering solubility solely in terms of the Hansen parameters neglects the important contributions of electrostatics to the solubility of the $PC_4$-TFSI. However, lacking a rigorous framework to model the phase behaviour, in the following we will treat proximity to the phase boundary in Fig. 2 as a measure of solvent quality.

### B. Scattering behaviour

**High dielectric constant solvents ($\epsilon \simeq 30 - 180$)**

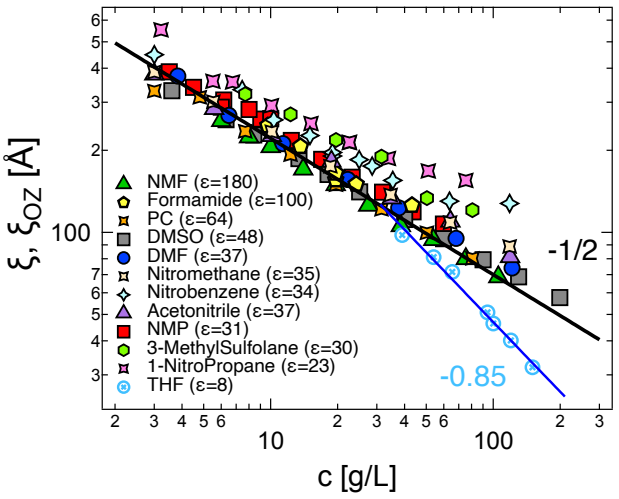


FIG. 3. Correlation length of PIL as a function of concentration solvents with $\epsilon \geq 30$ and in THF ($\epsilon \simeq 8$). Black line is scaling prediction of $\xi \propto c^{-1/2}$ and blue line is a best-fit power-law to THF data ($\xi_{OZ} = 290c^{-0.85}$), where $c$ is in g/L.

We begin by considering solvents with dielectric constants with $\epsilon > 30$, corresponding to 'high' dielectric constant solvents. Methanol solutions ($\epsilon = 32$) are discussed in the next section as their properties have more in common with those of solvents with intermediate permittivities. The scattering pattern for all solvents with $\epsilon > 30$ displayed a clear peak, and Eq. 5 was used to extract the correlation length, which is plotted as a function of polymer concentration for several solvents in Fig. 3. The exponent of $\xi \propto c^{-1/2}$ predicted by Eq. 3 is observed to broadly hold for the various solvents considered in Fig. 3. Slight deviations to higher values of $\xi$ are observed for high concentrations, in line with the reports for other polyelectrolytes in aqueous solutions.[34,35]

For the solvents considered in Fig. 3, the parameter $B$ is calculated by fitting eq. 3 with $b = 0.25$ nm. The results are plotted as a function of the Bjerrum length in Fig. 4. Two regions can be distinguished: For $l_B \lesssim 10$ Å , a constant value of $B \simeq 1.6$ is observed. Formamide ($l_B \simeq 6$ Å) is an exception, probably because it is a poor solvent, as evidenced from the fact that the $PC_4$-TFSI becomes insoluble for $c \gtrsim 50 - 60$ g/L, despite its high dielectric constant. For $l_B \gtrsim 10$Å , a power-law of $B \propto l_B^{1.3}$ is observed. This value can be compared with the exponents predicted by Eq. 4. If Manning condensation is assumed ($A \propto l_B$ ), the strongest exponent is for the poor solvent case with $B \propto l_B^{2/3}$, which is significantly lower than the value observed here.

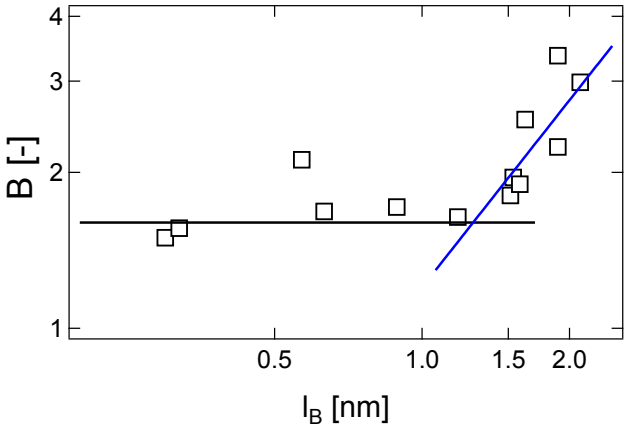


FIG. 4. Stretch parameter as a function of Bjerrum length of solvent. Flat line is guide to the eye. Blue line is best-fit power-law to data with $l_B > 1$ nm. The datum at $l_B \simeq 21$Å , B $\simeq 3$ is for a 50/50 wt% mixture of EGME and DMF. The dielectric constant of the mixed solvent was estimated as a volume average of that of the two solvents.

The regime with $B \sim l_B^0$ may correspond to the point at which $l_B \simeq l_K$. In this regime, the scaling model expects $B \simeq 1$ independent of $l_B$,[36] in fair agreement with our results. The exponent observed in the high $l_B$ region is inconsistent with Eq. 4 if Manning condensation ($A \propto l_B$) is assumed, as the strongest exponents expected is $B \propto l_B^{2/3}$ in the poor solvent case. It seems plausible that a change in the local chain conformation will itself influence the degree of counterion condensation, so that $A$ is a function of both $l_B$ and $B$. The simplest assumption we can make is to re-normalise $b$ to an effective monomer size of $b/B$. Then $A \sim l_B B$ is expected and $B \propto l_B$ for the theta solvent case is in fair agreement with our results.

### Intermediate dielectric constant solvents

We next consider solvents with $10 \lesssim \epsilon \lesssim 32$. Solutions in these solvents displayed either peaks or shoulders in their scattering function (except pyridine solutions ($\epsilon \simeq 12$), which are considered in the next section) . Solutions in methanol, acetone, benzaldehyde, 3-pentanone and 2-pentanone, displayed a peak in their scattering function at low concentrations. These become broader as the concentration increases and eventually morph into a shoulder. For 1-nitropropane we did not observe this transition, probably because we did not study sufficiently high concentrations. Solutions in t-BAA, MIBK and TEP displayed shoulders throughout the entire concentration range. The absence of peaks in lower dielectric constant solvents is qualitatively consistent with the scaling theory, which expects peaks to be visible only when there is more than one dissociated charge per correlation blob.

Figure 5a plots the correlation length as a function of concentration for several solvents in this range. Full symbols correspond to samples where the correlation length was extracted from the position of the peak and hollow symbols to solutions where the correlation length was extracted from the position of the shoulder. A power-law of $\xi \propto c^{-1/3}$, indicated by the full lines, is approximately observed for all solvents. Dobrynin and Rubinstein[9] predicted that polyelectrolytes with solvophobic backbones can, under certain conditions collapse into pearl-necklace structure, where dense globules (pearls) are connected by highly stretched sections of the chain (strings). Several predictions of this model were validated by the experimental work of Boue and co-workers.[37–42] In the bead dominated regime, the scaling of the correlation length is expected to be $\xi \propto c^{-1/3}$, matching our experimental observations.

**Origin of solvophobic forces:** The theory of Dobrynin and Rubinstein expects that solvophobic collapse is promoted by unfavourable polymer-solvent interactions and lower effective charge density. This is broadly consistent with our experimental observations, where the $\xi \propto c^{-1/3}$ scaling is only observed for solvents with $\epsilon \lesssim 23$. The exception to this is methanol, which based on it's proximity to the non-soluble region in 2 is expected to be a poorer solvent than the others considered. However, it is unclear why all 10 solvents with $\epsilon \lesssim 23$, which have very different chemical structures and are located in different regions of the Hansen solubility sphere, should be poor solvents for the backbone. Schiessel and Pincus[43,44] have noted that as the Bjerrum length increases, dipolar attractions become more important, because 1) the number density of dipoles along the chain increases as more counterions condense and 2) the strength of attraction scales as $\sim l_B^2$.

Dipolar attraction modifies the intrinsic (non-electrostatic) excluded volume parameter, lowering the effective solvent quality. Assuming athermal solvent conditions, the non-electrostatic excluded volume is $v_0 \simeq b^3$. If there is one charged group per monomer, as is the case for our system, Schiessel and Pincus predict the effective excluded volume of the system to:

$$v \simeq b^3 - (1-f) f b l_B^2 \qquad (7)$$

where $f$ is the fraction of free counterions.

According to Eq. 7, the effective excluded volume of polyelectrolytes in an athermal solvent for the backbone becomes negative when:

$$l_B \gtrsim b/\sqrt{f(1-f)}$$

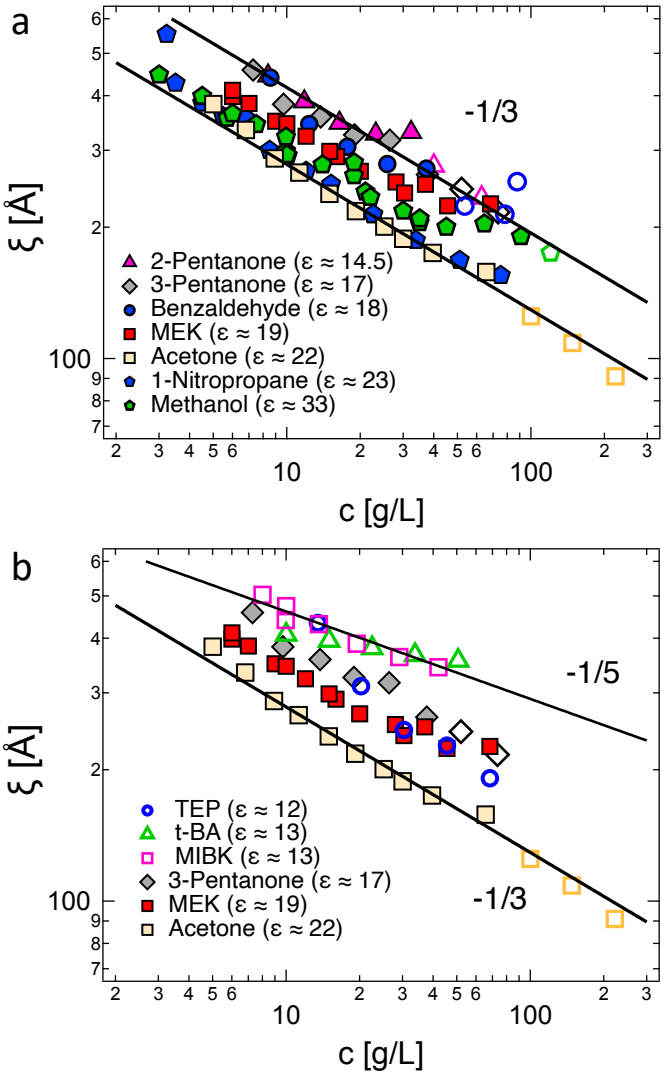


FIG. 5. Correlation length of PIL as a function of concentration for solvents with $12 \geq \epsilon \geq 32$. Full symbols are for solutions where the correlation length is extracted from the peak position and hollow symbols for those where it is extracted from the shoulder position. a) Black lines are scaling prediction of $\xi \propto c^{-1/3}$ for solvopobic polyelectrolytes in the bead-controlled regime. b) Data for acetone, MEK and 3-pentanone are the same as in part a. The other three solvents did not show peaks over the entire concentration range studied.

According to the Oosawa-Manning condensation theory, $f \simeq b/l_B$. As the Bjerrum length approaches the monomer size, $f \simeq 1$ and the above inequality is not satisfied. When $l_B \gg b$, we can approximate $1 - f \simeq 1$, and the criterion for poor solvent conditions becomes $l_B \gtrsim b$. This is clearly met for all solvents in figure 5. This simple calculation provides a basis to explain why many solvents of different chemical structures appear to act as poor solvents for PC4-TFSI.[45]

**Properties of pearl-necklaces:** Setting aside the question of the origin of solvophobic forces, we next examine the properties of the polyelectrolyte chains using the theory of Dobrynin and Rubinstein. If most of the polymer mass is contained in the beads, the correlation length can be calculated from the mean inter-bead distance as:

$$\xi = g_b^{1/3} c^{-1/3} \tag{8}$$

where $g_b$ is the number of chemical monomers inside a bead, predicted by the scaling model to be:

$$g_b \simeq \tau b/(f^2 l_B) \tag{9}$$

where $f$ is the fraction of monomers bearing a dissociated charge and $\tau$ is the reduced temperature. For poor solvents far below the theta temperature $\tau \simeq 1$.

Equation 8 was used to calculate the number of monomers per bead in the various solvents plotted in figure 5a. The results are listed in table II and plotted as a function of the Bjerrum length in figure 6, where a dependence of $g_b \sim l_B^3$ is observed if the methanol datum, which is unusual in that it is very close to the solubility boundary in the Hansen map, is excluded. The scaling model expects counterion condensation to take place inside the beads if $g_b > D_b/l_B$, which is satisfied for all the solvents if the beads are assumed to contain $> 0.1$wt% polymer. If Oosawa-Manning condensation holds, Eq. 9 gives $g_B \sim l_B$, which is weaker than the scaling law observed in 6. A possible way to reconcile the results in figure 6 and Eq. 9 is to assume that the solvent quality increases with increasing Bjerrum length. This appears unlikely as the influence of dipoles or charge correlations becomes increasingly strong as $l_B$ increases, thereby lowering the effective solvent quality of the system.

As noted above, above a solvent-dependent critical concentration ($c_B$), the solutions in fig. 5 display a shoulder instead of a correlation peak. A possible reason for this is that at $c_B$ the beads begin to overlap, and therefore, no inter-bead correlation peak occurs. We note that other phenomena such as increased counterion condensation could also explain the disappearance of the peak. If we proceed with the bead overlap hypothesis, the volume fraction of polymer inside the beads is $\phi_B \simeq c_B v_P$, where $v_P$ is the partial molar volume of the monomer. The values of $\phi_b$ are listed in table II and take values of $\simeq 0.02 - 0.05$. According to the scaling model, $\phi_B \simeq \tau$, which would indicate that the solvent quality is significantly worse for acetone, MEK and methanol than for benzaldehyde, 2-pentanone and 3-pentanone. This is not consistent with the Hansen solubility map in fig. 2, which expects methanol to be a worse solvent than MEK and acetone.

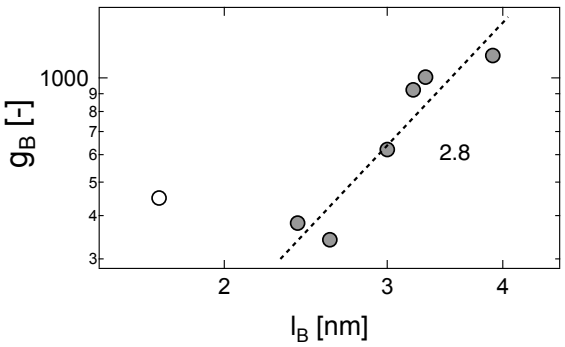


FIG. 6. Number of monomers in the beads of the pearl-necklace as a function of Bjerrum length of the solvent. Calculated by fitting eq. 9 to the data in figure 5a. We assume $\tau = 1$ for all solvents. Methanol datum is shown as hollow circle. Line is a power-law of $g_B \simeq 22 l_B^3$, fitted to the data excluding methanol.

| Solvent | $l_B$ [nm] | $g_b$ | $D_b^{\phi=1}$ [nm] | $\phi_b$ |
|---|---|---|---|---|
| MeOH | 1.7 | 451 | 5.7 | 0.058 |
| 1-Nitropropane | 2.4 | 381 | 1.9 | – |
| Acetone | 2.6 | 341 | 2.5 | 0.052 |
| MEK | 3.0 | 621 | 1.7 | 0.050 |
| Benzaldehyde | 3.2 | 924 | 1.8 | 0.019 |
| 3-Pentanone | 3.3 | 1005 | 2.6 | 0.023 |
| 2-pentanone | 3.9 | 1161 | 2.1 | 0.028 |

TABLE II. Properties of pearl-necklace beads calculated from Eq. 8.

Data for the correlation length of MIBK and t-BAA display weaker exponents of $\xi \sim c^{-(0.15-0.2)}$. Triethyl phosphate, despite having a similar dielectric constant displays the scaling of $\xi \sim c^{-1/3}$ observed for solvents in fig 5. Similarly weak concentration dependencies of the correlation length were reported by Waigh et al for another poly(ionic liquid) in poor solvent solutions.[46]

#### Low dielectric constant solvents (THF and pyridine)

The concentration scaling of equation 3 is a case of the more general scaling law derived by de Gennes:

$$\xi \simeq R(c^*)\Big(\frac{c}{c^*}\Big)^{-\nu/(3\nu-1)} \tag{10}$$

where $R(c^*)$ is the end-to-end distance of a chain at the overlap concentration $c^*$ and $\nu$ is the solvent quality exponent, which related the chain size $R$ to the degree of polymerisation ($N$) in dilute solution as: $R \propto N^{\nu}$.

Equation 10 expects $\xi \propto c^{-0.78}$ for neutral polymers if the thermal blob size is smaller than the correlation

length (good solvent regime) and $\xi \propto c^{-1}$ when the correlation blob is smaller than the thermal blob (concentrated or $\theta$ solvent regime). The data for THF solutions displays a value in between these two exponents, somewhat closer to the good solvent case.

The scaling theory expects the osmotic pressure of polymers in good solvent to be proportional to the number density of correlation blobs in semidilute good solvent solutions:[29,30]

$$\Pi = \frac{k_B T}{\xi_\Pi^3} \tag{11}$$

where the subscript $\Pi$ is added to note that this correlation length is expected to proportional but not equal to that extracted from scattering measurements.[30,32,47]

For theta solvents, where the osmotic pressure is not set by the density of binary contacts between chains, the $\Pi \propto \xi^{-3}$ is not expected to apply, but it is still possible to use Eq. 11 to define an osmotic correlation length from the osmotic pressure as $\xi_\Pi = \sqrt[3]{\Pi/k_B T}$.

The zero angle total structure factor $[S(q)]$ of two-component mixtures is given by:[48]

$$S(0) = k_B T \phi \frac{d\phi}{d\Pi} \tag{12}$$

where $\phi$ is the polymer volume fraction of polymer.

The scattering intensity is proportional related to the structure factor as $I(q) = [\frac{b_s}{v_s} - \frac{b_p}{v_p}]^2 S(q)$, where $b$ and $v$ are the coherent scattering length and volume of the solvent ($s$) and repeating unit of the polymer ($p$). Combining Eqs. 10-12, the following scaling law is obtained for the zero-angle scattering intensity:

$$I(0) \propto c^{(3\nu-2)/(3\nu-1)} \tag{13}$$

Figure 7 plots the dependence of the correlation length and zero angle scattering intensity for solutions in THF. Equations 10-13 are plotted for $\nu = 0.59$ ($c \leq 75$ g/L) and $\nu = 0.5$ ($c > 75$ g/L). This behaviour is expected for a neutral polymer in good solvent with a cross-over to the concentrated regime at $c^{**} = 75$ g/L, where the chain becomes Gaussian on all lengthscales above the Kuhn segment. Interestingly, despite the low dielectric constant of the solvents, dipolar attraction and/or charge-charge correlations are not important for this system, presumably due to the high degree of charge delocalisation in the counterions.

**The osmotic correlation length:** The zero angle scattering intensity, which is known in absolute units for the SANS measurements, can be used to evaluate the osmotic compressibility ($\phi \frac{d\phi}{d\Pi}$)[49] of the solutions, from which the osmotic correlation length can be calculated. From the data in the semidilute regime ($c < c^{**}$) we fit Eq. 12 with $\Pi = Ac^{2.3}$, where the exponent corresponds to the theoretical value from Eqs. 10 and 11 with $\nu = 0.59$ and the pre-factor is left as a free parameter. This yields $\xi_{OZ}/\xi_\Pi \simeq 3.4$, which is close to the value calculated by Huang and Witten[47] for polystyrene in Toluene ($\xi_\Pi/\xi_{OZ} = 3.6$). The result shows the negligible contribution of counterions to the osmotic pressure and further highlights the neutral polymer character of $PC_4TFSI$ in THF. In the concentrated regime ($c > c^{**}$), we use $\Pi = Ac^3$, as predicted by the scaling model for neutral polymers in theta solvents.[29,50] The ratio between scattering and osmotic correlation lengths takes a slightly larger value of $\xi_{OZ}/\xi_\Pi \simeq 3.7$, in contrast to polystyrene solutions in theta solvent, where it takes a lower value of 3.

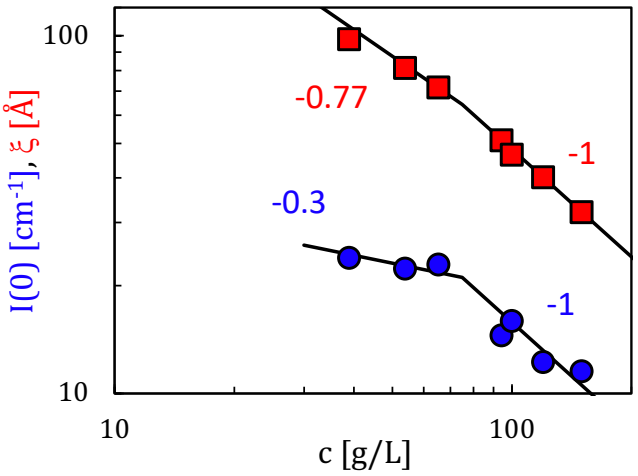


FIG. 7. Correlation length and zero-angle scattering intensity obtained from eq. 6 as a function of polymer concentration for solutions in THF. Lines are best fit power-laws to Eqs 10 and 13 with $\nu = 0.59$ for $c \leq 75$ g/L and $\nu = 0.5$ for $c > 75$ g/L. The overlap concentration, assessed viscosimetrically is $c^* \simeq 24$ g/L.

**Estimating the thermal blob size in THF solutions:** The cross-over in exponents observed in Figure 7 allows us to make a an estimate for the size of the thermal blob size of the PIL in THF: For polystyrene a comparison of dilute $R_g$ data for toluene and cyclohexane solutions gives an end-to-end distance for the thermal blob of $\xi_T \simeq 6.4$ nm. SANS data indicate the correlation length in d-toluene solution at $c = c^{**} \simeq 0.35$ g/mL is $\xi(c^{**}) = 0.7$ nm. Assuming a constant ratio of $\xi_T/\xi(c^{**}) \simeq 9$, we estimate the thermal blob for the $PC_4$-TFSI to be $\xi_T \simeq 57$ nm. If a Kuhn length of 2 nm, typical for flexible polymers is assumed, the number of monomers in the thermal blob is calculated to give: $g_{\xi,T} = 6600$.[51]

**Application of the Random Phase Approximation:** The structure factor of a polymer solution is predicted by the RPA to be:

$$\frac{1}{S(q)} = \frac{1}{\phi v_p N P(q)} + \frac{1}{v_s(1-\phi)} - \frac{2\chi}{v_s} \tag{14}$$

where $P(q)$ is the form factor of the chains (normalised to P(0) = 1) and $\chi$ is the Flory-Huggins solubility pa-

| $c$ [g/L] | $\xi$ [nm] | $I(0)$ [cm$^{-1}$] | $\chi$ [-] |
|---|---|---|---|
| 39 | 97.8 | 15.9 | 0.507 |
| 54 | 81.1 | 14.9 | 0.511 |
| 65 | 71.6 | 15.2 | 0.515 |
| 94 | 50.9 | 9.7 | 0.522 |
| 100 | 46.3 | 10.6 | 0.524 |
| 120 | 40.2 | 8.1 | 0.529 |
| 150 | 32.0 | 7.7 | 0.539 |

TABLE III. Fit parameters for $PC_4TFSI$ in THF solutions. Correlation length and $I(0)$ are obtained from Eq. 6.

rameter. For Gaussian chains in the $qR_g < 1$ limit, Eq. 14 is equivalent to Eq. 6 with $\xi = \sqrt{R_g^2/(2\phi N v_p)}$ and $S(0) = [\frac{1}{v_s 1-\phi} - \frac{2\chi}{v_s}]^{-1}$. The fitted $\xi$ and $I(0)$ values along with the calculated $\chi$ are listed in table III. A value of $R_g^2/N \simeq 16$Å$^2$, corresponding to a Kuhn length of $\simeq 39$ Å.

For $q^2R_g^2/N \gg 1$, equation 14 expects the structure factor to be proportional to the form factor of the polymer. In the semidilute regime, $P(q)$ is expected to scale display a cross-over between $P(q) \propto q^{-1.7}$ for $1 \gtrsim qR_g \gtrsim 4/l_K$ and $P(q) \propto q^{-1}$ at high $q$ is observed. In the intermediate $q$ region, our data display $S(q) \propto q^{-1.7\pm0.1}$ even for $c > 75$ g/L, which appears to be inconsistent with our assumption that this concentration corresponds to a cross-over to the concentrated regime. It is possible that the observed exponents are the result of a broad a cross-over between $q^{-2}$ at low $q$ and $q^{-1}$ at high $q$.

Fits to the pyridine data are considered in the supporting information. In brief, at low concentrations, solutions display a shoulder, the position of which decreases with increasing concentration. At higher concentrations, Ornstein-Zernike behaviour is observed. The correlation length and zero-angle scattering intensity increase with concentration, suggesting the system approaches a phase boundary.

## VI. CONCLUSIONS

We have studied the solubility and scattering properties of a poly(ionic liquid) with hydrophobic counterions in different organic solvents. Polar aprotic solvents were found to dissolve the polymer, while non-polar or protic solvents generally did not. The solubility could be described by using the Hansen parameter approach. Three types of behaviour were observed in the scattering data (peak, shoulder and Ornstein-Zernike), which were assigned to the relative importance of electrostatic, attractive and excluded volume interactions.

In the extended polyelectrolyte regime, which we observe for solvents with $\epsilon \gtrsim 30$, the correlation length scales as $\xi \sim c^{-1/2}$. The degree of local chain folding was quantified via the stretching parameter, which was shown to depend on the Bjerrum length when $l_B \gtrsim 1$ nm. The observed scaling $B \sim l_B^{1.3}$ does not match the scaling prediction, perhaps due to a subtle interplay between the local chain conformation and the degree of counterion condensation.

For solvents of intermediate dielectric constant, the correlation length scales as $\xi \sim c^{-1/3}$, which suggests chains are in partially collapsed (pearl necklace) conformation. Using the Dobyrnin-Rubinstein model, the mass per bead and bead volume fraction is estimated, and a correlation of these parameters with he solvent's Bjerrum length is established.

In THF, the scattering profiles and the scaling of the correlation length and zero-angle scattering suggests that the PIL behaves like a neutral polymer. Interestingly, despite the low dielectric constant of the solvent and the density of charged groups along the backbone, the solution properties do not appear to be controlled by dipolar attraction, as is the case in ionomers.

These results highlight the complex behaviour of polymerised ionic liquids in solution. Our further work will focus on understanding the influence of dielectric constant on counterion condensation and correlating the scattering and viscosity properties of PILs.

## VII. AUTHOR'S CONTRIBUTIONS

**Funding Acquisition:** TW, AM, CGL, WR. **Beam time proposals:** TW, CGL, CH, WR. **Data Fitting:** AG. **PIL synthesis:** AM. **Phase Mapping experiments:** CGL, TW, AM. **Scattering experiments:** CGL, TW, AM, AG, CH, HO, YT, YM, KF. **Data interpretation and analysis:** CGL, TW, AM. All authors contributed to the writing of the final version of the manuscript.

## ACKNOLEDGEMENTS

This work was supported by JSPS KAKENHI Grant Numbers 20KK0325. CGL acknowledges support from the DFG (grant GO 3250/2-1) and the Theodore von Karman scholarship provided by RWTH. The DFG grant RI 560/26-1 partially funded this research. We thank JPARC, ISIS, Spring-8 and the Diamond Light Source for providing beamtime for the scattering experiments. The neutron experiment at the Materials and Life Science Experimental Facility of the J-PARC was performed under a user program (Proposal No. 2022A0029 and 2022B0101). We thank Hiroki Iwase (TAIKAN), Sarah Rogers and Leidi Cavalcanti (SANS2D), Diego Alba Venero (ZOOM), Noburu Ohta (BL40b2) and Thomas Zinn (I22) for their assistance with the scattering experiments and data reduction. We also thank Max Hohenschutz for his assistance during our beam time at I22. Furthermore, we thank Steven Abbott for providing us with the data for Hansen Solubility Parameters of the solvents used.

## VIII. REFERENCES


[1]R. Hayes, G. G. Warr, and R. Atkin, "Structure and nanostructure in ionic liquids," Chem. Rev. **115**, 6357–6426 (2015), pMID: 26028184, https://doi.org/10.1021/cr500411q.

[2]N. Nishimura and H. Ohno, "15th anniversary of polymerised ionic liquids," Polymer **55**, 3289–3297 (2014), polymerized Ionic Liquids.

[3]T. Watanabe, E. Oe, Y. Mizutani, and T. Ono, "Toughening of poly(ionic liquid)-based ion gels with cellulose nanofibers as a sacrificial network," Soft Matter **19**, 2745–2754 (2023).

[4]U. H. Choi, T. L. J. Price, D. V. Schoonover, H. W. Gibson, and R. H. Colby, "The effect of oligo(oxyethylene) moieties on ion conduction and dielectric properties of norbornene-based imidazolium tf2n ionic liquid monomers," Macromolecules **53**, 4990–5000 (2020).

[5]D. Burgess, N. Li, N. Rosik, P. J. Fryer, I. McRobbie, H. Zhang, and Z. J. Zhang, "Surface-grafted poly(ionic liquid) that lubricates in both non-polar and polar solvents," ACS Macro Letters **10**, 907–913 (2021), pMID: 34306821.

[6]A. Wilke, J. Yuan, M. Antonietti, and J. Weber, "Enhanced carbon dioxide adsorption by a mesoporous poly(ionic liquid)," ACS Macro Letters **1**, 1028–1031 (2012), pMID: 35607031.

[7]Y. Zhang, B. Wang, E. H. M. Elageed, L. Qin, B. Ni, X. Liu, and G. Gao, "Swelling poly(ionic liquid)s: Synthesis and application as quasi-homogeneous catalysts in the reaction of ethylene carbonate with aniline," ACS Macro Letters **5**, 435–438 (2016), pMID: 35607225.

[8]K. Prabhu Charan, N. Pothanagandhi, K. Vijayakrishna, A. Sivaramakrishna, D. Mecerreyes, and B. Sreedhar, "Poly(ionic liquids) as "smart" stabilizers for metal nanoparticles," European Polymer Journal **60**, 114–122 (2014).

[9]A. V. Dobrynin and M. Rubinstein, "Hydrophobic polyelectrolytes," Macromolecules **32**, 915–922 (1999).

[10]A. Gulati, M. Jacobs, C. G. Lopez, and A. V. Dobrynin, "Salt effect on the viscosity of semidilute polyelectrolyte solutions: Sodium polystyrenesulfonate," Macromolecules **56**, 2183–2193 (2023).

[11]H. Chen and Y. A. Elabd, "Polymerized ionic liquids: Solution properties and electrospinning," Macromolecules **42**, 3368–3373 (2009), https://doi.org/10.1021/ma802347t.

[12]A. Matsumoto, F. Del Giudice, R. Rotrattanadumrong, and A. Q. Shen, "Rheological scaling of ionic-liquid-based polyelectrolytes in ionic liquid solutions," Macromolecules **52**, 2759–2771 (2019).

[13]A. Matsumoto, R. Yoshizawa, O. Urakawa, T. Inoue, and A. Q. Shen, "Rheological scaling of ionic liquid-based polyelectrolytes in the semidilute unentangled regime from low to high salt concentrations," Macromolecules **54**, 5648–5661 (2021), https://doi.org/10.1021/acs.macromol.1c00576.

[14]A. Matsumoto and A. Q. Shen, "Rheological scaling of ionic-liquid-based polyelectrolytes in ionic liquid solutions: the effect of the ion diameter of ionic liquids," Soft Matter **18**, 4197–4204 (2022).

[15]R. M. Fuoss and U. P. Strauss, "The viscosity of mixtures of polyelectrolytes and simple electrolytes," Ann. N. Y. Acad. Sci. **51**, 836–851 (1949).

[16]A. V. Dobrynin, R. H. Colby, and M. Rubinstein, "Scaling theory of polyelectrolyte solutions," Macromolecules **28**, 1859–1871 (1995).

[17]A. V. Dobrynin and M. Rubinstein, "Theory of polyelectrolytes in solutions and at surfaces," Prog. Polym. Sci. **30**, 1049–1118 (2005).

[18]D. C. Boris and R. H. Colby, "Rheology of sulfonated polystyrene solutions," Macromolecules **31**, 5746–5755 (1998).

[19]C. G. Lopez, "Scaling and entanglement properties of neutral and sulfonated polystyrene," Macromolecules **52**, 9409–9415 (2019).

[20]C. G. Lopez and W. Richtering, "Conformation and dynamics of flexible polyelectrolytes in semidilute salt-free solutions," J. Chem. Phys. **148**, 244902 (2018).

[21]C. G. Lopez, R. H. Colby, P. Graham, and J. T. Cabral, "Viscosity and scaling of semiflexible polyelectrolyte nacmc in aqueous salt solutions," Macromolecules **50**, 332–338 (2017).

[22]C. G. Lopez, "Entanglement of semiflexible polyelectrolytes: Crossover concentrations and entanglement density of sodium carboxymethyl cellulose," J. Rheol. **64**, 191–204 (2020).

[23]C. G. Lopez, "Entanglement properties of polyelectrolytes in salt-free and excess-salt solutions," ACS Macro Lett. **8**, 979–983 (2019).

[24]A. Matsumoto, R. Ukai, H. Osada, S. Sugihara, and Y. Maeda, "Tuning the solution viscosity of ionic-liquid-based polyelectrolytes with solvent dielectric constants via the counterion condensation," Macromolecules **55**, 10600–10606 (2022), https://doi.org/10.1021/acs.macromol.2c01405.

[25]R. Marcilla, J. A. Blazquez, R. Fernandez, H. Grande, J. A. Pomposo, and D. Mecerreyes, "Synthesis of novel polycations using the chemistry of ionic liquids," Macromol. Chem. Phys. **206**, 299–304 (2005), https://onlinelibrary.wiley.com/doi/pdf/10.1002/macp.200400411.

[26]G. S. Manning, "Limiting laws and counterion condensation in polyelectrolyte solutions i. colligative properties," J. Chem. Phys. **51**, 924–933 (1969), https://doi.org/10.1063/1.1672157.

[27]C. M. Hansen, *Hansen solubility parameters: a user's handbook* (CRC press, 2007).

[28]K. Salamon, D. Aumiler, G. Pabst, and T. Vuletic, "Probing the mesh formed by the semirigid polyelectrolytes," Macromolecules **46**, 1107–1118 (2013).

[29]M. Rubinstein and R. H. Colby, *Polymer Physics* (Oxford University Press: New York, 2003).

[30]W. W. Graessley, *Polymeric liquids & networks: structure and properties* (Garland Science, 2003).

[31]M. Daoud, J. Cotton, B. Farnoux, G. Jannink, G. Sarma, H. Benoit, C. Duplessix, C. Picot, and P. De Gennes, "Solutions of flexible polymers. neutron experiments and interpretation," Macromolecules **8**, 804–818 (1975).

[32]C. G. Lopez, F. Horkay, M. Mussel, R. L. Jones, and W. Richtering, "Screening lengths and osmotic compressibility of flexible polyelectrolytes in excess salt solutions," Soft matter **16**, 7289–7298 (2020).

[33]M. Spiteri, *Conformation et correÃÂlations spatiales dans les solutions de polyeÃÂlectrolytes: eÃÂtude par Diffusion de Neutrons aux Petits Angles*, Ph.D. thesis, Ph. D, Orsay, 1997 and Spiteri, MN (1997).

[34]K. Nishida, K. Kaji, and T. Kanaya, "High concentration crossovers of polyelectrolyte solutions," J. Chem. Phys. **114**, 8671–8677 (2001).

[35]P. Lorchat, I. Konko, J. Combet, J. Jestin, A. Johner, A. Laschewski, S. Obukhov, and M. Rawiso, "New regime in polyelectrolyte solutions," EPL (Europhysics Letters) **106**, 28003 (2014).

[36]The value of $B = 1$ is expected if the conformation inside the correlation blob is a rod-like array of electrostatic blobs. If a directed random-walk is assumed instead, $B > 1$ is expected.

[37]M. Spiteri, C. Williams, and F. Boué, "Pearl-necklace-like chain conformation of hydrophobic polyelectrolyte: a sans study of partially sulfonated polystyrene in water," Macromolecules **40**, 6679–6691 (2007).

[38]S. Ben Mahmoud, W. Essafi, A. Brulet, and F. Boue, "How necklace pearls evolve in hydrophobic polyelectrolyte chains under good solvent addition: A sans study of the conformation," Macromolecules **51**, 9259–9275 (2018).

[39]W. Essafi, M.-N. Spiteri, C. Williams, and F. Boué, "Hydrophobic polyelectrolytes in better polar solvent. structure and chain conformation as seen by saxs and sans," Macromolecules **42**, 9568–9580 (2009).

[40]W. Essafi, W. Raissi, A. Abdelli, and F. Boué, "Metastability of large aggregates and viscosity, and stability of the pearl necklace conformation after organic solvent treatment of aqueous hydrophobic polyelectrolyte solutions," J. Phys. Chem. B

**118**, 12271–12281 (2014).

[41] W. Essafi, A. Abdelli, G. Bouajila, and F. Boué, "Behavior of hydrophobic polyelectrolyte solution in mixed aqueous/organic solvents revealed by neutron scattering and viscosimetry," J. Phys. Chem. B **116**, 13525–13537 (2012).

[42] "One notable exception is the prediction that the specific viscosity scales with concentration as $\eta_{sp} \sim c^0$ in the bead controlled regime, which is not observed experimentally. For our solutions displaying $\xi \sim c^{-1/3}$ scaling, visual inspection also revealed an increase of the viscosity with concentration.".

[43] H. Schiessel and P. Pincus, "Counterion-condensation-induced collapse of highly charged polyelectrolytes," Macromolecules **31**, 7953–7959 (1998).

[44] H. Schiessel, "Counterion condensation on flexible polyelectrolytes: dependence on ionic strength and chain concentration," Macromolecules **32**, 5673–5680 (1999).

[45] Note that if Oosawa-Manning condensation holds, the $1 - f \simeq 1$ only introduces an error of $\lesssim 10\%$.

[46] T. A. Waigh, R. Ober, C. E. Williams, and J.-C. Galin, "Semidilute and concentrated solutions of a solvophobic polyelectrolyte in nonaqueous solvents," Macromolecules **34**, 1973–1980 (2001), https://doi.org/10.1021/ma001086j.

[47] J.-R. Huang and T. A. Witten, "Universal ratios of characteristic lengths in semidilute polymer solutions," Macromolecules **35**, 10225–10232 (2002).

[48] J. S. Higgins and H. C. Benoit, "Polymers and neutron scattering," (1994).

[49] Note that other definitions are used for the term osmotic compressibility in the scattering literature, here we follow the notation of Graessley, who defines it by analogy to the isothermal compressibility.

[50] R. H. Colby, "Structure and linear viscoelasticity of flexible polymer solutions: comparison of polyelectrolyte and neutral polymer solutions," Rheol. Acta **49**, 425–442 (2010).

[51] Note that poly(ionic liquids) are different from neutral polymers because in that bulk state, chains are not in the $\theta$ condition.[52].

[52] L. N. Wong, S. D. Jones, K. Wood, L. De Campo, T. Darwish, M. Moir, H. Li, R. A. Segalman, G. G. Warr, and R. Atkin, "Polycation radius of gyration in a polymeric ionic liquid (pil): the pil melt is not a theta solvent," Physical Chemistry Chemical Physics **24**, 4526–4532 (2022).